International Journal of Cardiology 275 (2019) 179–186

Contents lists available at ScienceDirect

International Journal of Cardiology

journal homepage: www.elsevier.com/locate/ijcard

CMR imaging biosignature of cardiac involvement due to cancer-related treatment by T1 and T2 mapping

Jasmin D. Haslbauer [a], Sarah Lindner [b], Silvia Valbuena-Lopez [a,c], Hafisyatul Zainal [a,d], Hui Zhou [a,e], Tommaso D'Angelo [a,f], Faraz Pathan [a,g], Christophe A. Arendt [a,h], Gesine Bug [b], Hubert Serve [b], Thomas J. Vogl [h], Andreas M. Zeiher [i], Gerry Carr-White [j], Eike Nagel [a], Valentina O. Puntmann [a,i,j,*,1]

[a] Institute of Experimental and Translational Cardiac Imaging, DZHK Centre for Cardiovascular Imaging, Goethe University Hospital Frankfurt, Frankfurt am Main, Germany
[b] Department of Haematology and Oncology, Goethe University Hospital Frankfurt, Frankfurt am Main, Germany
[c] Department of Cardiology, University Hospital La Paz, Madrid, Spain
[d] Department of Cardiology, Universiti Teknologi MARA (UiTM), Sg. Buloh, Malaysia
[e] Department of Radiology, XiangYa Hospital, Central South University, Changsha, Hunan, China
[f] Department of Biomedical Sciences and Morphological and Functional Imaging, G. Martino University Hospital Messina, Italy
[g] Department of Cardiology, Menzies Institute for Medical Research, University of Tasmania, Australia
[h] Department of Radiology, Goethe University Hospital Frankfurt, Frankfurt am Main, Germany
[i] Department of Cardiology, Goethe University Hospital Frankfurt, Frankfurt am Main, Germany
[j] Department of Cardiology, Guys and St Thomas' NHS Trust, London, United Kingdom

ARTICLE INFO

Article history:
Received 18 August 2018
Received in revised form 20 September 2018
Accepted 5 October 2018
Available online 11 October 2018

ABSTRACT

Background: Cancer-related treatment is associated with development of heart failure and poor outcome in cancer-survivors. T1 and T2 mapping by cardiovascular magnetic resonance (CMR) may detect myocardial injury due to cancer-related treatment.
Methods: Patients receiving cancer-related treatment regimes underwent screening of cardiac involvement with CMR, either within 3 months (early Tx) or >12 months (late Tx) post-treatment. T1 and T2 mapping, cardiac function, strain, ischaemia-testing, scar-imaging and serological cardiac biomarkers were obtained.
Results: Compared to age/gender matched controls (n = 57), patients (n = 115, age (yrs): median(IQR) 48(28-60), females, n = 60(52%) had reduced left ventricular ejection fraction (LV-EF) and strain, and higher native T1 and T2. The early Tx group (n = 52) had significantly higher native T1, T2 and troponin levels compared to the late Tx group, indicating myocardial inflammation and oedema ($p < 0.01$). On the contrary, late Tx patients showed raised native T1, increased LV-end-systolic volumes, reduced LV-EF and deformation, and elevated NT-proBNP, suggesting myocardial fibrosis and remodelling ($p < 0.05$). Prospective validation of these results in an independent cohort of patients with similar treatment regimens (n = 25) and longitudinal assessments revealed high concordance of CMR imaging signatures of early and late cardiac involvement.
Conclusions: Native T1 and T2 mapping can be valuable in detecting and monitoring of cardiac involvement with cancer-related treatment, providing distinct biosignatures of early inflammatory involvement (raised native T1 and T2) and interstitial fibrosis and remodelling (raised native T1 but not T2), respectively. Our findings may provide an algorithm allowing to identify susceptible myocardium to potentially guide cardio-protective treatment measures.

1. Introduction

Success of modern cancer treatments led to significantly improved overall survival from haemato-oncological conditions. Yet, improved outcome exposes a growing population of patients to increased cardiovascular (CV) morbidity and mortality, predominantly due to developing heart failure (HF) [1–3]. Cardiotoxic effects of older cytotoxic agents, such as anthracyclines, antimetabolites, taxanes and alkylating agents as well as radiotherapy, are well established. Newer targeted therapies such as tyrosine kinase inhibitors, anti-HER2 receptor blockers, antiangiogenic agents and checkpoint inhibitors have similarly been associated with cardiotoxic effects [1,4]. Although the exact mechanisms of cardiotoxic myocardial injury remain to be fully elucidated, the individual susceptibility to cardiotoxicity also plays a role, as demonstrated by a genetically-driven predilection to mount a more adverse

* Corresponding author at: Institute for Experimental and Translational Cardiovascular Imaging, DZHK Centre for Cardiovascular Imaging, Goethe University Frankfurt, University Hospital, Frankfurt am Main, Germany.
E-mail address: vppapers@icloud.com (V.O. Puntmann).
[1] This author takes responsibility for all aspects of the reliability and freedom from bias of the data presented and their discussed interpretation.

https://doi.org/10.1016/j.ijcard.2018.10.023
0167-5273/

cellular metabolism in response to anthracycline therapy, which is affecting only a subset of all patients [5]. Personalised approaches to recognition of early myocardial changes during the course of cancer therapies may help to detect and prevent the late consequences of cardiac involvement by guiding early prevention [6,7]. Studies reported globally reduced left ventricular (LV) ejection fraction (LV-EF), mainly on the account of enlarged end-systolic volume (LV-ESV). Additionally, reduced longitudinal deformation, impaired diastolic function and rise of serological cardiac biomarkers, including troponin and NT-proBNP have been reported [5–9]. Retrospective patient studies reported significantly elevated myocardial T1 mapping indices, sensitive and direct measures of diffusely abnormal myocardial involvement by cardiac magnetic resonance (CMR) [8–11]. These findings were corroborated in an experimental study with T1 and T2 mapping, further highlighting the role of early inflammatory involvement followed by diffuse fibrotic remodelling [12]. In this study, we investigated patients receiving cancer-related treatments within the first 3 months (early Tx) or >12 months prior (late Tx) for the phenotypical evidence of myocardial injury using CMR. We compared the findings, firstly to age-gender and CV risk factors matched controls, and secondly, to observations in an independent cohort of similar patients with longitudinal assessments.

2. Methods

One hundred and fifteen patients (≥18 years) without previously known or symptomatic cardiac disease were referred for screening of cardiac involvement due to cancer-related treatment from local oncology departments (London, n = 82, Frankfurt, n = 33, *the original cohort*). Non-exposed subjects, matched for age, gender and CV risk factor profile, with low pretest likelihood for cardiomyopathy or previous history of cardiac events or coronary artery disease, with no clinical or serological evidence for systemic inflammation, taking no anti-inflammatory medication, served as *controls* (n = 57). An independent cohort of patients underwent longitudinal assessments at 2, 12 and 18 months after receipt of treatment (n = 25, Frankfurt, *the longitudinal cohort*). The general contraindication to contrast-enhanced CMR were observed, including known allergy to gadolinium contrast agents, pregnancy, cochlear implants, cerebral aneurysm clips and non-CMR compatible pacemakers (no subject was excluded due to these contraindications in the present study). Clinical meta-data was recorded for all patients (Table 1). The study protocol was reviewed and approved by respective local ethics committees and written informed consent was obtained from all participants. All procedures were carried out in accordance with the Declaration of Helsinki.

2.1. Study procedures

All subjects underwent a standardised CMR protocol for routine assessment of cardiac volumes, mass, T1 and T2 mapping, myocardial perfusion and late gadolinium enhancement (LGE) [13,14], using 3-Tesla (T) scanners (Achieva, Philips Healthcare, Best, The Netherlands, and Skyra, Siemens Healthineers, Erlangen). In the longitudinal cohort, the serial follow-up assessments consisted of native T1 and T2 mapping and cardiac volumes only. Patients with symptoms and signs of systemic infection were not included. After standardised specific planning, volumetric cavity assessment was performed by whole-heart coverage of short-axis (SAX) slices. Myocardial mapping acquisitions were made in a single midventricular SAX slice using the investigator-specific modified Look-Locker Imaging (FFM-MOLLI) [15,16] for T1 mapping. A hybrid gradient and spin echo (GraSE) sequence [17,18] at the London site and T2-FLASH sequence [19,20] at the Frankfurt site for T2 mapping. All sequence types and parameters have been validated and published previously. Sequence-specific normal ranges were employed (FFM MOLLI native T1: 3.0-T: mean of the normal range 1052 ± 23 ms; i.e. upper limit of normal range: 1098 ms at 3.0-T) [21], native T2: GraSE sequence: 45 ± 4 ms [17], T2-FLASH sequence 35 ± 4 ms [19,22]. Myocardial perfusion imaging with adenosine infusion (140–210 μg/kg/min) with dynamic acquisition during administration of 0.1 mmol/kg body weight gadobutrol (Gadovist®, Bayer AG, Leverkusen, Germany) [23]. LGE was performed in a SAX stack ~15 min after contrast agent administration, using a mid-diastolic inversion prepared 2-dimensional gradient echo sequence (TE/TR/flip-angle 2.0 ms/3.4 ms/25°, acquired voxel size 1.4 × 1.4 × 8 mm) with individually adapted prepulse delay to achieve optimally nulled myocardium.

Cardiac volume and function were quantified using commercially available software (MEDIS®, Leiden) following standardised post-processing recommendations [24]. LGE was characterised as present or absent, and ischaemic or non-ischaemic in type, based on the predominant pattern. Quantitative tissue characterisation and myocardial deformation analysis was performed by the core-lab (Goethe CVI, Frankfurt), blinded to the underlying subject group allocation and the time-point of the examination. Native T1 and T2 were measured in the septal myocardium of the midventricular SAX using the ConSept approach, as previously described [25,26]. Areas of LGE were excluded from the mapping ROIs to avoid areas of regional replacement fibrosis. Global longitudinal and circumferential strain was measured using feature tracking [27]. Longitudinal deformation was averaged from 3 long-axis views, circumferential deformation from 3 SAX slices (apical, mid, basal); both are expressed as absolute global peak systolic strain. Venous blood sampling was performed immediately prior to the CMR study for analysis for high-sensitive Troponin T (hs-TropT), hs-C reactive protein (CRP) and N-terminal-pro brain natriuretic peptide (NT-proBNP) using commercially available test-kits (Elecsys 2010®, Roche, Basel, Switzerland). Analytical validation and limits of detection of the hs-TropT test were used to define normal/abnormal (≥13.9 ng/l) [28]. The cut off of 300 pg/l was used for a clinically relevant elevation of NT-proBNP [29].

2.2. Statistical analysis

Statistical analysis was performed using SPSS, version 24. Normality of distributions was tested using the Shapiro-Wilk test. Results are presented as counts (percentage) for categorical data, mean (SD) or median (interquartile range, IQR) for continuous data, as appropriate. Comparisons between groups were performed using Student *t*-test or one-Way ANOVA for normally distributed variables, and chi2 and Mann-Whitney test for non-normally distributed variables. The associations were analysed by uni- and multivariate regression analyses. Collinearity diagnostics was used to examine the variance inflation factor analysis. Inter- and intraobserver reproducibility and agreement of post-processing approaches have been reported previously [24,25,29,30]. All tests were two-tailed and p-values < 0.05 were considered statistically significant.

3. Results

Subject characteristics and results of blood markers are summarised in Table 1. Patients were similar to controls for age, gender, blood pressure, heart rate and CV risk profile (age (years): median (IQR) 48 (28–60), male, n = 60, 52%). Cancer diagnoses included haematological malignancies (acute myeloid leukaemia (n = 15, 13%), acute lymphoblastic leukaemia (n = 2, 2%), chronic myeloid leukaemia (n = 26, 23%), Hodgkin lymphoma (n = 6, 5%); non-Hodgkin lymphoma (n = 9, 8%), multiple myeloma (n = 9, 8%), and solid tumours, including breast cancer (n = 26, 22%), testicular (n = 6, 5%), prostatic cancer (n = 9, 8%), sarcoma (n = 5, 4%). Cancer-related treatments are listed in Table 1. Early and late Tx groups were similar in proportions of induction and adjuvant chemotherapy regimens, as well as radiation therapy (p = 0.481). Doxorubicin was the most commonly used anthracycline (n = 82, 71%), followed by daunorubicin (n = 14, 12%), epirubicin (n = 11, 10%) and mitoxantrone (n = 8, 7%). On average, patients received an equivalent doxorubicin dose of 181 mg/m^2 (60–330 mg/m^2). Compared to controls, patients had lower eGFR, haemoglobin/haematocrit, and significantly higher cardiac serological biomarkers (<0.001 for all). Twelve subjects (10%) had hs-TropT levels above the clinically significant threshold [28]. Only a minority of patients was treated for hypertension or received lipid-lowering therapy or had identifiable pre-existing heart disease (n = 19, 16% with LGE, see below).

CMR findings are summarised in Table 1. Global systolic impairment was more common in the late Tx group (impaired: defined as LV-EF ≤ 50% [30]; early vs. late Tx: n = 24, 46% vs. n = 42, 67%, p = 0.019; severely impaired: defined as LV-EF ≤ 35% [31]: n = 5, 9% vs. n = 18, 28%, p = 0.020). Compared to controls, late Tx group also had significantly reduced global longitudinal (GLS), but not global circumferential strain (GCS). Patients had significantly higher native T1 and T2 values compared to controls (p < 0.001) (Fig. 1S). Both groups had a similarly high prevalence of subjects with abnormal native T1 (~60%). Compared to the late Tx group, patients in the early Tx group had significantly higher native T1 (p < 0.05) and native T2 (p < 0.001).

3.1. Analysis of relationships

In the early Tx group, there was positive correlation between hs-TropT levels with native T1 and native T2 (Fig. 2S in Supplementary material) (p < 0.01 for all), but no relationship between NT-proBNP with native T1 (r = 0.145, p = 0.37). On the contrary, there was a linear relationship between NT-proBNP and native T1, GLS and LV-EF in the late Tx group (r = 0.271, r = 0.259, p < 0.05 for all), but not with hs-TropT (r = −0.181, p = 0.12). Results of binary logistic regression and ROC analyses on comparative ability of CMR measures (native T1

Table 1
Subjects' characteristics and CMR measurements of function and structure and tissue characterisation. One-way ANOVA, *t*-test or Fisher exact test; all tests were two-tailed, $p < 0.05$ was considered significant. GLS – global longitudinal strain, GRS – global radial strain, GCS – global circumferential strain, LGE – late gadolinium enhancement, SD – standard deviations; abnormal native T1, T2 and GLS defined as 2 SD from the mean of the normal range.

Variable	Controls (n = 57)	Patients (n = 115)	Sig. (p-value)
Age (years)	54 ± 17	59 ± 22	0.134
Male (n, %)	26 (46)	55 (48)	0.805
BMI (kg/m^2)	26 ± 5	25 ± 6	0.28
BP systolic (mm Hg)	131 ± 14	134 ± 21	0.331
BP diastolic (mm Hg)	73 ± 9	76 ± 12	0.097
Heart rate (bpm)	64 ± 10	66 ± 12	0.279
Smokers (n, %)	14 (25)	24 (21)	0.553
Hypertension (n, %)	11 (20)	18 (16)	0.514
Diabetes (n, %)	5 (10)	8 (7)	0.707
Hyperlipidaemia (n, %)	17 (30)	27 (23)	0.320
Blood haemoglobin (g/dl)	14.2 ± 1.2	11.6 ± 1.4	<0.001
Blood haematocrit (%)	44 ± 4	41 ± 6	<0.001
Estimated GFR (mL/min/m^2)	93 ± 11	84 ± 15	<0.001
hs-TropT, ng/l	2.24 (1.5–3.1)	6.9 (4.2–8.6)	<0.001
Abnormal hs-TropT (>13.9 ng/l, n (%))	0 (0)	12 (10)	<0.001
hs C-reactive protein, mg/l	2.4 ± 1.9	8.1 ± 3.8	<0.001
NT-proBNP (pg/l)	77 ± 44	243 ± 174	<0.001
>300, n (%)	(0)	31 (27)	<0.001
Anthracycline chemotherapy, n (%)	/	112 (97)	/
Induction, n (%)	/	60 (53)	/
Adjuvant, n (%)	/	52 (47)	/
Additional therapies			/
Anthraquinones, n (%)		23 (20)	/
Trastuzumab, n (%)	/	30 (26)	/
Taxanes, n (%)	/	41 (36)	/
Radiation, n (%)	/	65 (56)	/
Biological therapies[a], n (%)	/	30 (26)	/
Cardiac medication			
RAAS inhibitors, n (%)	11 (20)	18 (16)	0.604
Beta blockers, n (%)	9 (16)	14 (12)	0.468
Platelet inhibition, n (%)	2 (4)	11 (10)	0.172
Lipid-lowering therapy, n (%)	17 (30)	27 (23)	0.320

	Controls (n = 57)	Early Tx (n = 52)	Late Tx (n = 63)	Sig. (p-value)
LV-EDV index, mL/m^2	76 ± 12	82 ± 28[a]	101 ± 29[a]	<0.001
LV-ESV index, mL/m^2	29 ± 7	47 ± 26[a]	59 ± 27	<0.001
LV-EF (%)	60 ± 7	55 ± 11[a]	48 ± 12	<0.001
LV mass index (g/m^2)	52 ± 13	58 ± 14[a]	49 ± 12	0.001
RV-EF (%)	55 ± 9	50 ± 9[a]	50 ± 11[a]	0.008
LA area, cm^2	17 ± 4	16 ± 6	20 ± 7[a]	0.001
GLS (%)	24 ± 5	21 ± 8	17 ± 11[a]	<0.001
GCS (%)	29 ± 4	27 ± 8	27 ± 5	0.077
Myocardial LGE, n (%)	0 (0)	9 (18)	10 (16)	0.775
Ischaemic type, n (%)	/	4 (8)	5 (8)	
Non-ischaemic, n (%)	/	5 (10)	5 (8)	
LGE extent (%)	/	5.7 (2.5–8.9)	7.1 (1.7–12.6)	0.680
Myocardial ischaemia, n (%)	0 (0)	2 (3)	1 (2)	0.73
Pericardial enhancement, n (%)	/	2 (4)	3 (6)	0.627
Pericardial effusion, n (%)	/	15 (29)	16 (25)	0.630
Native T1 (msec)	1053 ± 21	1137 ± 61[a]	1121 ± 47[a]	<0.001
Abnormal native T1, n (%)	3 (4%)	36 (73)	52 (83)	0.822
Native T2 (msec, T2 GraSE, n = 118)	44 ± 3	50 ± 5[a]	46 ± 3[a]	0.004
Native T2 (msec, T2 Flash, n = 54)	34 ± 3	41 ± 3[a]	36 ± 3[a]	<0.001
Abnormal native T2, n (%)	0 (0)	16 (38)	7 (13)	0.004

[a] Biological therapies included imatinib, dasatinib, rituximab and lenalidomide.

and T2, LV-EF, LV-ESV, GLS, LGE and hs-TropT and NT-proBNP) to detect cardiac involvement in patients exposed to cancer-related treatment are presented in Table 2, Figs. 1 and 3S (in Supplementary material). Univariate and multivariate analyses (stepwise, forward likelihood ration, with adjustment for patients' demographics, CV risk factors and the equivalent doxorubicin dose) revealed native T1 to be the strongest independent discriminator of myocardial involvement in all patients as well as in the separate groups. Native T2 acted as the second most effective discriminator in the early Tx group, indicating that the presence of myocardial oedema is driving the change in native T1 [26,32]. In contrast, the late Tx group displayed a correlation between native T1 and GLS, but not native T2, indicating diffuse interstitial fibrotic remodelling [26,33].

We simulated the scenarios of clinical decision making by using binary variables based on established definitions of cardiac abnormalities (e.g. LGE present/absent; LV-EF ≤ 50%, GLS ≤ 17%, hs-TropT (13.9 ng/l) and NTproBNP (≥300 pg/l), as well as native T1 and T2 (normal/abnormal) on the predefined cut-offs of 2SD above the mean of normal range (see Methods). Native T1 (≥2SD) was the strongest discriminator between controls and all patients with exposure to cancer-related therapy, as well as the two subgroups, followed by native T2 (≥2SD) in the early Tx group, and GLS ≤ 17% in the late Tx group.

3.2. Imaging biosignature of cardiotoxicity

Based on these, we developed phenotypical signatures for early and late cardiac involvement after cancer-related treatment (early involvement: native T1 ≥ 2SD and native T2 ≥ 2SD; late involvement: native T1 > 2SD and normal T2 and/or GLS ≤ 17%). With this algorithm, cardiac

Table 2
Results of binary logistic regression and ROC curve analyses, using separate models with continuous and binary variables. AUC – area under the curve; CI – confidence interval, LH – likelihood ration, HR – hazard ratio.

Univariate analyses controls vs. all patients			Sig. (p-value)	Binary variables	AUC (95%CI)	Sig. (p-value)
Continuous variables	AUC (95%CI)	HR (95%CI)				
LV-EF (%)	0.78 (0.67–0.78)	0.89 (0.80–0.95)	<0.001	LV-EF ≤ 50%	0.76 (0.68–0.84)	<0.001
GLS (%)	0.84 (0.68–0.87)	0.84 (0.78–0.89)	<0.001	GLS ≤ 17%	0.80 (0.74–0.86)	<0.001
Native T1 (10 ms)	0.94 (0.87–0.95)	1.7 (1.5–1.1)	<0.001	Native T1 (≥2SD)	0.90 (0.85–0.93)	<0.001
Native T2 (AU)	0.72 (0.71–0.86)	1.5 (1.2–1.8)	<0.001	Native T2 (≥2SD)	0.62 (0.52–0.72)	0.026
LVmass (index, g/m^2)	0.53 (0.59–0.73)	1.2 (1.07–1.2)	<0.001	LGE (present)	0.50 (0.36–0.59)	0.960
hs-TropT (ng/l)	0.86 (0.80–0.93)	1.7 (1.4–2.1)	0.001	hs-TropT (≥13.9 ng/l)	0.54 (0.44–0.64)	0.414
NT-proBNP (10 pg/l)	0.83 (0.76–0.89)	1.2 (1.1–1.3)	0.003	NT-proBNP (≥300 pg/l)	0.63 (0.54–0.72)	0.011

Multivariate analyses	HR (95%CI)	Sig. (p-value)	Sensitivity (95%CI)	Specificity (95%CI)	Accuracy (95%CI)	NPV	PPV
Native T1 (10 msec)	1.7 (1.5–1.1)	<0.001	92 (87–95)	80 (67–88)	89 (82–94)	76 (64–86)	92 (88–96)

Adjusted for (p-value): GLS (0.001), LV-EF (0.028), native T2 (0.87), LV-ESV (index) (0.11), LV mass (index) (0.73), LGE (cat) (0.11), DoxEq (0.09), age (0.38), hypertension (0.35), diabetes, (0.73) hyperlipidemia (0.52), hs-CRP (0.31), hs-TropT (0.12), NT-proBNP (0.22)

Univariate analyses: controls vs. early Tx group

Continuous variables	AUC (95%CI)	HR (95%CI)	Sig. (p-value)	Binary variables	AUC (95%CI)	Sig. (p-value)
LV-EF (%)	0.75 (0.65–0.85)	0.91 (0.84–0.99)	0.001	LV-EF ≤ 50%	0.71 (0.59–0.82)	0.001
GLS (%)	0.77 (0.66–0.87)	1.8 (1.4–2.5)	0.001	GLS ≤ 17%	0.73 (0.61–0.78)	<0.001
Native T1 (10 msec)	0.91 (0.82–0.97)	1.6 (1.3–1.8)	<0.001	Native T1 (≥2SD)	0.87 (0.78–0.95)	<0.001
Native T2 (AU)	0.85 (0.76–0.93)	1.9 (1.5–2.5)	<0.001	Native T2 (≥2SD)	0.81 (0.77–0.85)	<0.001
LV-mass (index) (g/m^2)	0.50 (0.37–0.64)	1.01 (0.99–1.02)	0.484	LGE (present)	0.53 (0.41–0.66)	0.58
hs-TropT (ng/l)	0.83 (0.74–0.91)	1.4 (1.2–1.7)	0.001	hs-TropT (≥13.9 ng/l)	0.61 (0.50–0.73)	0.066
NT-proBNP (10 pg/l)	0.81 (0.71–0.89)	1.2 (1.1–1.3)	0.001	NT-proBNP (≥300 pg/l)	0.58 (0.46–0.70)	0.119

Multivariate analyses	HR (95%CI)	Sig. (p-value)	Sensitivity (95%CI)	Specificity (95%CI)	Accuracy (95%CI)	NPV	PPV
Model 1							
Native T1 (10 msec)	1.6 (1.3–1.1)	<0.001	78 (71–91)	86 (78–90)	88 (81–91)	78 (69–88)	85 (79–90)

Adjusted for (p-value): GLS (0.04), LV-EF (0.29), native T2 (0.01), LV-ESV (index) (0.96), LV mass (index) (0.27), LGE (cat) (0.33), DoxEq (0.02), age (0.44), hypertension (0.41), diabetes, (0.79) hyperlipidemia (0.72), hs-CRP (0.42), hs-TropT (0.08), NT-proBNP (0.12)

Model 2							
Native T1 (10 msec)	1.7 (1.4–1.11)	<0.001	98 (89–99)	94 (85–96)	96 (89–96)	97 (89–99)	93 (85–95)
Native T2 (AU)	1.5 (1.1–2.5)	0.001					

Adjusted for (p-value): GLS (0.06), LV-EF (0.34), LV-ESV (index) (0.46), LV mass (index) (0.42), LGE (cat) (0.58), DoxEq (0.04), age (0.64), hypertension (0.63), diabetes, (0.91) hyperlipidemia (0.77), hs-CRP (0.63), hs-TropT (0.08), NT-proBNP (0.12)

Univariate analyses: controls vs. late Tx group

Continuous variables	AUC (95%CI)	HR (95%CI)	Sig. (p-value)	Binary variables	AUC (95%CI)	Sig. (p-value)
LV-EF (%)	0.80 (0.73–0.88)	0.84 (0.76–0.87)	0.001	LV-EF ≤ 50%	0.80 (0.73–0.88)	<0.001
GLS (%)	0.88 (0.83–0.94)	0.71 (0.62–0.79)	<0.001	GLS ≤ 17%	0.85 (0.78–0.92)	<0.001
Native T1 (msec)	0.96 (0.93–0.99)	2.1 (1.6–2.4)	<0.001	Native T1 (abnormal)	0.91 (0.86–0.97)	<0.001
Native T2 (AU)	0.65 (0.55–0.75)	1.3 (1.1–1.6)	0.008	Native T2 (abnormal)	0.57 (0.46–0.68)	0.052
LV-mass (index) (g/m^2)	0.56 (0.46–0.67)	1.02 (1.0–1.04)	0.056	LGE (present)	0.49 (0.38–0.60)	0.870
hs-TropT (ng/l)	0.88 (0.77–0.92)	1.9 (1.5–2.4)	0.001	hs-TropT (≥13.9 ng/l)	0.50 (0.29–0.61)	0.991
NT-proBNP (10 pg/l)	0.85 (0.78–0.92)	1.2 (1.1–1.3)	0.001	NT-proBNP (≥300 pg/l)	0.65 (0.56–0.75)	0.004

Multivariate analyses	HR (95%CI)	Sig. (p-value)	Sensitivity (95%CI)	Specificity (95%CI)	Accuracy (95%CI)	NPV	PPV
Model 1							
Native T1 (10 msec)	1.1 (1.1–1.2)	<0.001	89 (83–94)	84 (73–91)	89 (80–93)	82 (73–89)	91 (85–96)

Adjusted for (p-value): GLS (0.001), LV-EF (0.042), native T2 (0.87), LV-ESV (index) (0.02), LV mass (index) (0.59), LGE (cat) (0.12), DoxEq (0.21), age (0.41), hypertension (0.25), diabetes, (0.51) hyperlipidemia (0.48), hs-CRP (0.53), hs-TropT (0.17), NT-proBNP (0.52)

Model 2							
Native T1 (10 msec)	1.1 (1.6–1.2)	<0.001	93 (87–96)	89 (78–95)	92 (84–96)	89 (79–95)	93 (88–97)
GLS (%)	0.77 (0.67–0.87)	0.003					

Adjusted for (p-value): LV-EF (0.29), native T2 (0.52), LV-ESV (index) (0.14), LV mass (index) (0.29), LGE (cat) (0.09), DoxEq (0.39), age (0.21), hypertension (0.25), diabetes, (0.42) hyperlipidemia (0.34), hs-CRP (0.77), hs-TropT (0.39), NT-proBNP (0.64)

abnormalities were found in 88 (76%) of all exposed patients (in contrast to 3 (4%) of controls), resulting in a detection rate (by way of diagnostic accuracy) of 84% (Chi^2 74, $p < 0.01$). In comparison, abnormalities based on GLS (≤17%), LV-EF (≤50%), hs-TropT [28] and NT-proBNP were found in 71%, 66%, 61% and 48% respectively. Prospective testing of this algorithm in an independent cohort of subjects undergoing cancer-related treatment, fulfilling identical inclusion criteria for age, gender and CV risk profile ($n = 25$) with longitudinal assessments (2, 12 and 18 months) achieved similar results and corroborated the temporal evolution of imaging findings in a longitudinal observation (Fig. 2). In the longitudinal group, native T1 levels at 2 months were inversely associated with LV-EF at 18 months (LV-EF18, $r = -401$, $p = 0.042$) and delta LV-EF (2–18 months, $r = 0.52$, $p = 0.001$). Linear regression analyses (stepwise, including the measures at 2 months: native T1 and T2, hs-tropT and NT = proBNP) revealed predictive association between native T1 at 2 months and LV-EF at 18 months (per 10 ms change B - 0.75 (−0.2–0.03) and delta LV-EF (2–18 months) (HR per 10 ms - 0.75 (−0.2–0.03).

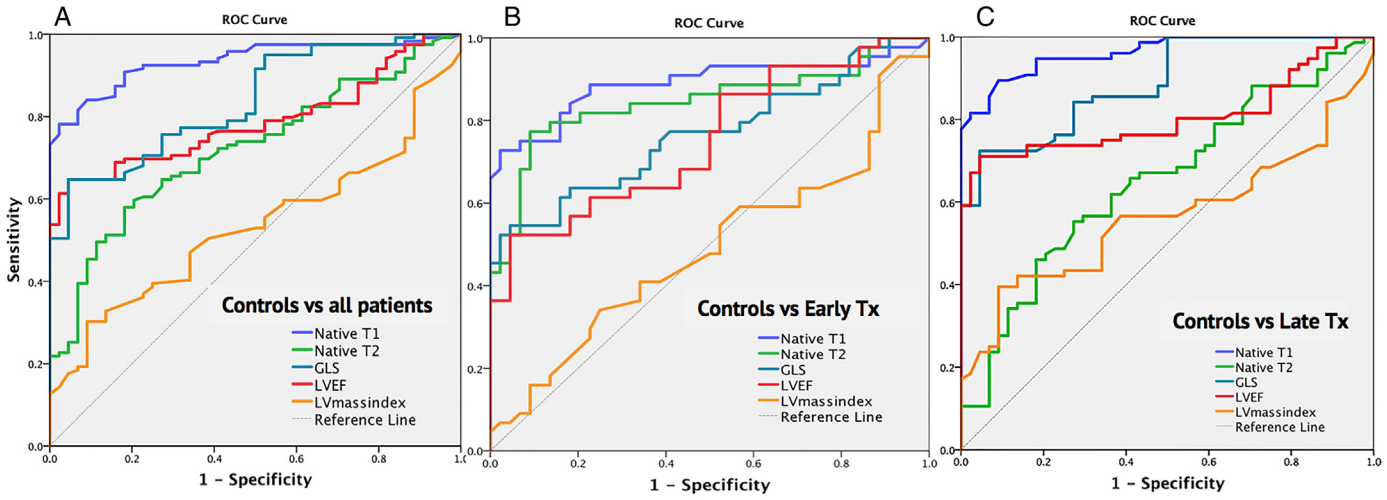

Fig. 1. ROC curve analysis of native T1, T2, GLS, LV-EF and LVmass (index) comparing Controls with All (A), Early Tx (B) and Late Tx (C) Cohorts. Native T1 showed the highest diagnostic accuracy to detect cardiac involvement between controls and all patients (panel A). In the analysis between controls and early Tx, similar results are observed with native T1 and T2 showing the highest values in sensitivity (panel B). However, in the late Tx group, T2 sensitivity is less prominent, consistent with the pathophysiological findings that myocardial oedema subsides at a later stage post treatment. Native T1 holds the highest diagnostic accuracy in this cohort (panel C). GLS = global longitudinal strain, LV-EF = left ventricular ejection fraction, LVmass (index) = left ventricular mass index.

4. Discussion

We demonstrate that native T1 and T2 mapping are valuable tools to characterise the pathophysiological myocardial changes in patients receiving cancer-related treatment. Firstly, compared to the non-exposed controls, native T1 was raised in a large majority of patients, irrespective of their group allocation. In patients with recent exposure, the rise in native T1 was stronger and accompanied by increased native T2, indicating myocardial oedema and inflammation (Fig. 2). In patients with past treatment, increased native T1 was paralleled by reduction in GLS and a rise in NT-proBNP, concordant with myocardial impairment with interstitial fibrosis [26,34]. Based on these results, we derived a biosignature of early and late cardiac involvement, based on native T1 and T2, and native T1 and GLS respectively, with high concordance of findings in an independent cohort of similar patients with longitudinal assessments. Head-to-head comparisons with established markers of cardiac injury and impairment, including serological markers, lent further support in validating the signals of non-invasive imaging measures in the context of exposure to cancer-related treatment.

The results of our study corroborate a number of previous reports on cancer-treatment and cardiac involvement, including the high rate of (mild-moderate) global systolic impairment, increase in T1 mapping indices and serological markers of myocardial injury. We expand the previous insights by employing T1 and T2 mapping, novel imaging methods to measure diffuse myocardial inflammation and fibrosis supported by a vast body of evidence, including in cancer survivors (summarised in [34,35]). Our findings are new and important, as they highlight the distinct phenotypical imaging signatures due to cancer-related treatment, which are differential in patients with recent and past exposure. Inflammatory myocardial injury is the hallmark of the early cardiac involvement, evidenced by raised native T1 and T2 [32,36]. On the contrary, the past exposure is characterised by diffuse myocardial interstitial fibrosis (abnormal native T1, but not T2) [26] and remodelling (reduced GLS and increased LV-ESV). Both signatures are further corroborated by the parallel rise in hs-TropT and NT-proBNP, serological markers of myocardial injury and LV stretch due to cardiac decompensation respectively. Thus, a non-invasive imaging signature with a direct relationship to the underlying pathophysiology may have an ability to detect and monitor the presence and severity of disease. Native T1 is sensitive to the presence of abnormal myocardium and reacts to both pathophysiological substrates, myocardial fibrosis and oedema [26,32,37]. On the other hand, T2 mapping is water-specific, marking pathological states of myocardial oedema and inflammation [36,38]. Thus, the combination of these two imaging markers may help to inform on the pathophysiological drivers of myocardial tissue signal change, as either predominantly early inflammatory injury (raised native T1 and T2) or late interstitial fibrotic remodelling (raised native T1 and normal native T2). Structural and functional LV remodelling is more pronounced in the advanced late Tx group [39–41]; in earlier stages, small changes in remodelling measures are potentially difficult to discern [1,30], as they are preload-dependent and masked through a commonly encountered depletion of intravascular volume. Consequently, serological markers such as troponin and NT-proBNP is often utilised to help clarifying the presence of cardiac injury [40,42]. We provide an insight into the dynamics of serological biomarkers alongside the phenotypical characterisation of cardiac involvement. Compared to non-exposed controls, both markers are significantly elevated in response to cancer treatment, acting as predictive univariate discriminators of treatment exposure. Yet, their biochemical levels rarely reach beyond the clinically define thresholds of 13.9 ng/l for hs-TropT and 300 pg/l for NT-proBNP [28,29] of a 'positive' test. As such, their discriminatory performance is poor when clinical thresholds are applied. Historically, the thresholds were determined with the intent of supporting emergency room scenarios of either coronary artery occlusion or acute congestive HF [29–31]. In contrast, myocardial injury due to cancer-related treatment is mild, yet sustained, as evidenced by the persistently elevated troponin levels in a subclinical range [40,42]. Whereas there may be a scope for adjusting the biomarker thresholds and limits of detection to the context of cardiotoxic injury, further studies are required to establish such sensitivity/specificity ranges [30]. There is a noticeable wide spread of native T1 and T2 values and troponin levels in the early stage (Fig. 5), communicating heterogeneity of responses to injury. These are potentially reflecting the individual differences in susceptibility [5] or intensity of inflammatory/reparatory responses, as well as the variety of pathophysiological effects of different drug modalities [43], further explaining the difficulty of capturing the relevant signals unless sufficiently sensitive diagnostic methods, such as T1 and T2 mapping, are used [44]. The overall paucity of LGE reiterates the diffuse and global nature of the myocardial injury due to cancer-related treatment, with overall low prevalence of ischaemic-type scarring [24]. Still, scar imaging using LGE and ischaemia-testing by myocardial perfusion provide valuable clinical information on pre-existing cardiac conditions, which are known to importantly predispose to a worse outcome [1], perhaps better utilised ahead of cancer-

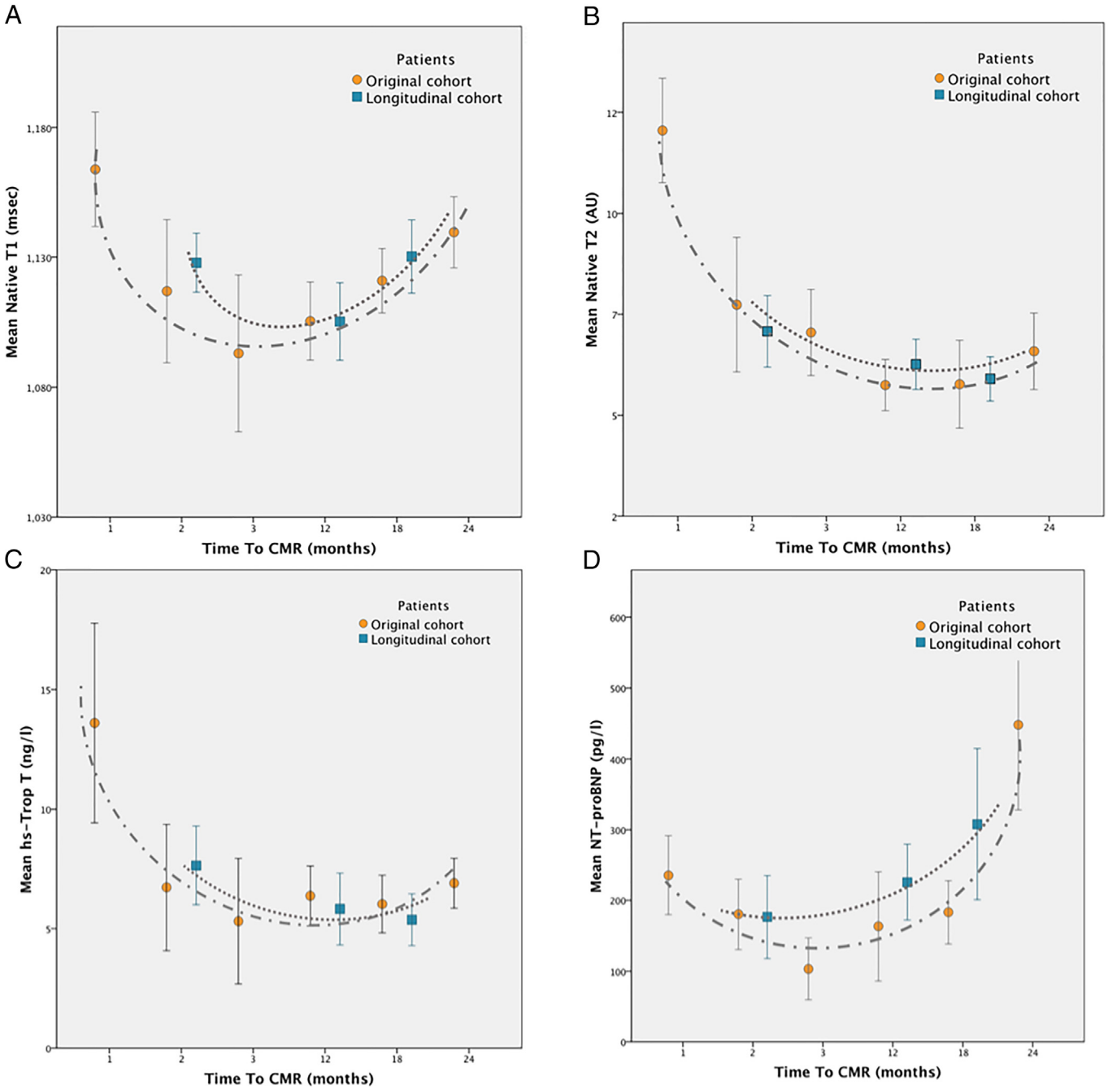

Fig. 2. Temporal evolution of measurements longitudinal cohort (n = 25) and comparison with the original cohort (n = 115). Native T1 values display in early months after receiving cancer-related therapies, dropping to lower values approximately 3 months post-therapy in both longitudinal and original cohorts. They then steadily increase 12–24 months after treatment, further confirming the involvement of fibrotic remodelling. In contrast, high native T2 values are observed in early stages post treatment (1 month), only to decrease steadily over time in both cohorts. The dynamics of T2 values are mirrored by hs-Trop T, while the serological changes NT-proBNP over time develop in synergy with T1 values.

treatment, facilitating the initiation of cardiac prevention or intervention. Because of the essentially myocardial effects of cancer-related treatment, the comprehensive screening for pre-existing disease, including assessment of baseline native T1 and T2 values and GLS, which is over and above the focus of anatomical CAD by the coronary angiography is essential [30,45]. Although ischaemic heart disease featured sparingly in our cohort, myocardial stress testing is a sufficiently low-risk add-on, to be offered systematically in most patients prior to cancer-therapy. We see this as an efficient way to reducing the burden of radiation and over-investigation, as well as exposure to kidney-damaging contrast agents in a patient population that is likely to receive many radiation-heavy diagnostic tests, adding to their cumulative exposure dose. Based on our findings, we propose a systematic approach of a comprehensive baseline CMR examination *prior to the start of cancer treatment*, followed by longitudinal assessments with T1 and T2 mapping (Fig. 5S in Supplementary material). Modern short imaging protocols allow for diagnostically reliable and clinically meaningful information, and may support identification of patients with susceptible myocardium [13]. Further studies are required to determine whether patients would benefit from cardio-protective treatment measures, as well as the intervention guided by T1 and T2 mapping would also improve the overall outcome.

A few limitations apply. In this study, the proof-of concept findings of a larger cohort of consecutive patients were validated in a smaller

independent group with longitudinal assessments. We believe that comparison of two cohorts provides important insights into the temporal evolution of cardiac injury due to cancer-related treatment. Validation in larger independent patient collectives would further strengthen our findings. The high sensitivity of T1 mapping to detect myocardial abnormality in the present study is partially explained by the choice of a T2-sensitive MOLLI sequence [26], as well as our postprocessing approach [25], allowing for a comparatively higher effect size in detection of abnormal myocardium [34]. Sequence parameters and validation have been previously published in several multicentre based-publications, confirming their reproducibility and transferability beyond an expert centre [15,21,45].

5. Conclusions

Native T1 and T2 mapping can be valuable in detecting and monitoring of cardiac involvement with cancer-related treatment, providing distinct biosignatures of early inflammatory involvement (raised native T1 and T2) and interstitial fibrosis and remodelling (raised native T1 but not T2), respectively. Our findings may provide an algorithm allowing to identify susceptible myocardium to potentially guide cardio-protective treatment measures, supporting personalised medicine.

Acknowledgements

We would like to acknowledge the support of cardiac radiographers, local cardiology departments at participating centres, and Philips and Siemens clinical scientists.

Disclosures of conflicts of interest

None.

Funding

Department of Health via the National Institute for Health Research (NIHR) comprehensive Biomedical Research Centre (BRC) award to Guy's & St Thomas' NHS Foundation Trust, King's College London and King's College Hospital NHS Foundation Trust. German Ministry of Education and Research via the German Centre for Cardiovascular Research (DZHK) to VP, AZ, EN.

Appendix A. Supplementary data

Supplementary data to this article can be found online at https://doi.org/10.1016/j.ijcard.2018.10.023.

References

[1] J.L. Zamorano, P. Lancellotti, D. Rodriguez Muñoz, et al., 2016 ESC Position Paper on cancer treatments and cardiovascular toxicity developed under the auspices of the ESC Committee for Practice Guidelines, Eur. Heart J. 37 (36) (2016) 2768–2801, https://doi.org/10.1093/eurheartj/ehw211.
[2] D.B. Sawyer, X. Peng, B. Chen, L. Pentassuglia, C.C. Lim, Mechanisms of anthracycline cardiac injury: can we identify strategies for cardioprotection? Prog. Cardiovasc. Dis. 53 (2) (2010) 105–113, https://doi.org/10.1016/j.pcad.2010.06.007.
[3] J.V. McGowan, R. Chung, A. Maulik, I. Piotrowska, J.M. Walker, D.M. Yellon, Anthracycline chemotherapy and cardiotoxicity, Cardiovasc. Drugs Ther. 31 (1) (2017) 63–75, https://doi.org/10.1007/s10557-016-6711-0.
[4] D. Jain, R.R. Russell, R.G. Schwartz, G.S. Panjrath, W. Aronow, Cardiac complications of Cancer therapy: pathophysiology, identification, prevention, treatment, and future directions, Curr. Cardiol. Rep. 19 (5) (2017) 36, https://doi.org/10.1007/s11886-017-0846-x.
[5] P.W. Burridge, Y.F. Li, E. Matsa, et al., Human induced pluripotent stem cell-derived cardiomyocytes recapitulate the predilection of breast cancer patients to doxorubicin-induced cardiotoxicity, Nat. Med. 22 (5) (2016) 547–556, https://doi.org/10.1038/nm.4087.
[6] G. Gulati, S.L. Heck, A.H. Ree, et al., Prevention of cardiac dysfunction during adjuvant breast cancer therapy (PRADA): a 2 × 2 factorial, randomized, placebo-controlled, double-blind clinical trial of candesartan and metoprolol, Eur. Heart J. 37 (21) (2016) 1671–1680, https://doi.org/10.1093/eurheartj/ehw022.
[7] D. Cardinale, A. Colombo, G. Bacchiani, et al., Early detection of anthracycline cardiotoxicity and improvement with heart failure therapy, Circulation 131 (22) (2015) 1981–1988, https://doi.org/10.1161/CIRCULATIONAHA.114.013777.
[8] J.H. Jordan, S. Vasu, T.M. Morgan, et al., Anthracycline-associated T1 mapping characteristics are elevated independent of the presence of cardiovascular comorbidities in cancer survivors, Circ. Cardiovasc. Imaging 9 (8) (2016), e004325. https://doi.org/10.1161/CIRCIMAGING.115.004325.
[9] T.G. Neilan, O.R. Coelho-Filho, R.V. Shah, et al., Myocardial extracellular volume by cardiac magnetic resonance imaging in patients treated with anthracycline-based chemotherapy, Am. J. Cardiol. 111 (5) (2013) 717–722, https://doi.org/10.1016/j.amjcard.2012.11.022.
[10] E.B. Tham, M.J. Haykowsky, K. Chow, et al., Diffuse myocardial fibrosis by T1-mapping in children with subclinical anthracycline cardiotoxicity: relationship to exercise capacity, cumulative dose and remodeling, J. Cardiovasc. Magn. Reson. 15 (1) (2013) 48, https://doi.org/10.1186/1532-429X-15-48.
[11] G.C. Meléndez, W.G. Hundley, Is myocardial fibrosis a new frontier for discovery in cardiotoxicity related to the administration of anthracyclines? Circ. Cardiovasc. Imaging 9 (12) (2016), e005797. https://doi.org/10.1161/CIRCIMAGING.116.005797.
[12] H. Farhad, P.V. Staziaki, D. Addison, et al., Characterization of the changes in cardiac structure and function in mice treated with anthracyclines using serial cardiac magnetic resonance imaging, Circ. Cardiovasc. Imaging 9 (12) (2016), e003584. https://doi.org/10.1161/CIRCIMAGING.115.003584.
[13] S. Valbuena-López, R. Hinojar, V.O. Puntmann, Cardiovascular magnetic resonance in cardiology practice: a concise guide to image acquisition and clinical interpretation, Rev. Esp. Cardiol. Engl. Ed. 69 (2) (2016) 202–210, https://doi.org/10.1016/j.rec.2015.11.011.
[14] C.M. Kramer, J. Barkhausen, S.D. Flamm, et al., Standardized cardiovascular magnetic resonance (CMR) protocols 2013 update, J. Cardiovasc. Magn. Reson. 15 (1) (2013) 91, https://doi.org/10.1186/1532-429X-15-91.
[15] D.R. Messroghli, A. Radjenovic, S. Kozerke, D.M. Higgins, M.U. Sivananthan, J.P. Ridgway, Modified Look-Locker inversion recovery (MOLLI) for high-resolution T1 mapping of the heart, Magn. Reson. Med. 52 (1) (2004) 141–146, https://doi.org/10.1002/mrm.20110.
[16] V.O. Puntmann, G. Carr-White, A. Jabbour, et al., T1-mapping and outcome in nonischemic cardiomyopathy, JACC Cardiovasc. Imaging 9 (1) (2016) 40–50, https://doi.org/10.1016/j.jcmg.2015.12.001.
[17] F. Bönner, N. Janzarik, C. Jacoby, et al., Myocardial T2 mapping reveals age- and sex-related differences in volunteers, J. Cardiovasc. Magn. Reson. 17 (1) (2015) 9, https://doi.org/10.1186/s12968-015-0118-0.
[18] R. Fernández-Jiménez, J. Sánchez-González, J. Agüero, et al., Fast T2 gradient-spin-echo (T2-GraSE) mapping for myocardial edema quantification: first in vivo validation in a porcine model of ischemia/reperfusion, J. Cardiovasc. Magn. Reson. 17 (1) (2015) 652, https://doi.org/10.1186/s12968-015-0199-9.
[19] S. Giri, Y.-C. Chung, A. Merchant, et al., T2 quantification for improved detection of myocardial edema, J. Cardiovasc. Magn. Reson. 11 (1) (2009) 56, https://doi.org/10.1186/1532-429X-11-56.
[20] D. Verhaert, P. Thavendiranathan, S. Giri, et al., Direct T2 quantification of myocardial edema in acute ischemic injury, JACC Cardiovasc. Imaging 4 (3) (2011) 269–278, https://doi.org/10.1016/j.jcmg.2010.09.023.
[21] D. Dabir, N. Child, A. Kalra, et al., Reference values for healthy human myocardium using a T1 mapping methodology: results from the International T1 Multicenter cardiovascular magnetic resonance study, J. Cardiovasc. Magn. Reson. 16 (1) (2014) 34, https://doi.org/10.1186/s12968-014-0069-x.
[22] B. Baeßler, F. Schaarschmidt, C. Stehning, B. Schnackenburg, D. Maintz, A.C. Bunck, A systematic evaluation of three different cardiac T2-mapping sequences at 1.5 and 3T in healthy volunteers, Eur. J. Radiol. 84 (11) (2015) 2161–2170, https://doi.org/10.1016/j.ejrad.2015.08.002.
[23] E. Nagel, Magnetic resonance perfusion measurements for the noninvasive detection of coronary artery disease, Circulation 108 (4) (2003) 432–437, https://doi.org/10.1161/01.CIR.0000080915.35024.A9.
[24] J. Schulz-Menger, D.A. Bluemke, J. Bremerich, et al., Standardized image interpretation and post processing in cardiovascular magnetic resonance: Society for Cardiovascular Magnetic Resonance (SCMR) Board of Trustees Task Force on Standardized Post Processing, J. Cardiovasc. Magn. Reson. 15 (1) (2013) 35, https://doi.org/10.1186/1532-429X-15-35.
[25] T. Rogers, D. Dabir, I. Mahmoud, et al., Standardization of T1 measurements with MOLLI in differentiation between health and disease – the ConSept study, J. Cardiovasc. Magn. Reson. 15 (1) (2013) 78, https://doi.org/10.1186/1532-429X-15-78.
[26] N. Child, G. Suna, D. Dabir, et al., Comparison of MOLLI, shMOLLLI, and SASHA in discrimination between health and disease and relationship with histologically derived collagen volume fraction, Eur. Heart J. Cardiovasc. Imaging 119 (2017) 277, https://doi.org/10.1093/ehjci/jex309.
[27] P. Claus, A.M.S. Omar, G. Pedrizzetti, P.P. Sengupta, E. Nagel, Tissue tracking technology for assessing cardiac mechanics, JACC Cardiovasc. Imaging 8 (12) (2015) 1444–1460, https://doi.org/10.1016/j.jcmg.2015.11.001.
[28] E. Giannitsis, K. Kurz, K. Hallermayer, J. Jarausch, A.S. Jaffe, H.A. Katus, Analytical validation of a high-sensitivity cardiac troponin T assay, Clin. Chem. 56 (2) (2010) 254–261, https://doi.org/10.1373/clinchem.2009.132654.
[29] J.L. Januzzi, R. van Kimmenade, J. Lainchbury, et al., NT-proBNP testing for diagnosis and short-term prognosis in acute destabilized heart failure: an international pooled analysis of 1256 patients: the International Collaborative of NT-proBNP Study, Eur. Heart J. 27 (3) (2006) 330–337, https://doi.org/10.1093/eurheartj/ehi631.
[30] J.C. Plana, M. Galderisi, A. Barac, et al., Expert consensus for multimodality imaging evaluation of adult patients during and after cancer therapy: a report from the American Society of Echocardiography and the European Association of

Cardiovascular Imaging, Eur. Heart J. Cardiovasc. Imaging 15 (10) (2014) 1063–1093, https://doi.org/10.1093/ehjci/jeu192.
[31] P. Ponikowski, A.A. Voors, S.D. Anker, et al., 2016 ESC Guidelines for the diagnosis and treatment of acute and chronic heart failure, Eur. Heart J. 37 (27) (2016) 2129–2200, https://doi.org/10.1093/eurheartj/ehw128.
[32] P. Lurz, C. Luecke, I. Eitel, et al., Comprehensive cardiac magnetic resonance imaging in patients with suspected myocarditis, J. Am. Coll. Cardiol. 67 (15) (2016) 1800–1811, https://doi.org/10.1016/j.jacc.2016.02.013.
[33] V.O. Puntmann, T. Voigt, Z. Chen, et al., Native T1 mapping in differentiation of normal myocardium from diffuse disease in hypertrophic and dilated cardiomyopathy, JACC Cardiovasc. Imaging 6 (4) (2013) 475–484, https://doi.org/10.1016/j.jcmg.2012.08.019.
[34] V.O. Puntmann, E. Peker, Y. Chandrashekhar, E. Nagel, T1 mapping in characterizing myocardial disease, Circ. Res. 119 (2) (2016) 277–299, https://doi.org/10.1161/CIRCRESAHA.116.307974.
[35] A.J. Taylor, M. Salerno, R. Dharmakumar, M. Jerosch-Herold, T1 mapping, JACC Cardiovasc. Imaging 9 (1) (2016) 67–81, https://doi.org/10.1016/j.jcmg.2015.11.005.
[36] R. Hinojar, L. Foote, S. Sangle, et al., Native T1 and T2 mapping by CMR in lupus myocarditis: disease recognition and response to treatment, Int. J. Cardiol. 222 (2016) 717–726, https://doi.org/10.1016/j.ijcard.2016.07.182.
[37] R. Hinojar, L. Foote, E. Arroyo Ucar, et al., Native T1 in discrimination of acute and convalescent stages in patients with clinical diagnosis of myocarditis, JACC Cardiovasc. Imaging 8 (1) (2015) 37–46, https://doi.org/10.1016/j.jcmg.2014.07.016.
[38] S. Bohnen, U.K. Radunski, G.K. Lund, et al., Performance of T1 and T2 mapping cardiovascular magnetic resonance to detect active myocarditis in patients with recent-onset heart failure, Circ. Cardiovasc. Imaging 8 (6) (2015), e003073–3. https://doi.org/10.1161/CIRCIMAGING.114.003073.
[39] J.H. Jordan, R.B. D'Agostino, C.A. Hamilton, et al., Longitudinal assessment of concurrent changes in left ventricular ejection fraction and left ventricular myocardial tissue characteristics after administration of cardiotoxic chemotherapies using T1-weighted and T2-weighted cardiovascular magnetic resonance, Circ. Cardiovasc. Imaging 7 (6) (2014) 872–879, https://doi.org/10.1161/CIRCIMAGING.114.002217.
[40] B.C. Drafts, K.M. Twomley, R. D'Agostino, et al., Low to moderate dose anthracycline-based chemotherapy is associated with early noninvasive imaging evidence of subclinical cardiovascular disease, JACC Cardiovasc. Imaging 6 (8) (2013) 877–885, https://doi.org/10.1016/j.jcmg.2012.11.017.
[41] T.G. Neilan, D. Pena-Herrera, O.R. Coelho-Filho, M. Jerosch-Herold, J. Moslehi, R. Kwong, Left ventricular mass by cardiac magnetic resonance imaging and adverse cardiovascular outcomes in patients treated with anthracycline-based chemotherapy, J. Cardiovasc. Magn. Reson. 14 (Suppl. 1) (2012) O30, https://doi.org/10.1186/1532-429X-14-S1-O30.
[42] D. Cardinale, M.T. Sandri, A. Colombo, et al., Prognostic value of troponin I in cardiac risk stratification of cancer patients undergoing high-dose chemotherapy, Circulation 109 (22) (2004) 2749–2754, https://doi.org/10.1161/01.CIR.0000130926.51766.CC.
[43] R.J. Gertz, T. Lange, J.T. Kowallick, et al., Inter-vendor reproducibility of left and right ventricular cardiovascular magnetic resonance myocardial feature-tracking, in: V. Lionetti (Ed.), PLoS One, vol. 13(3), , 2018, e0193746. https://doi.org/10.1371/journal.pone.0193746.
[44] F. Grothues, G.C. Smith, J.C.C. Moon, et al., Comparison of interstudy reproducibility of cardiovascular magnetic resonance with two-dimensional echocardiography in normal subjects and in patients with heart failure or left ventricular hypertrophy, Am. J. Cardiol. 90 (1) (2002) 29–34, https://doi.org/10.1016/S0002-9149(02)02381-0.
[45] V.O. Puntmann, G. Carr-White, A. Jabbour, et al., Native T1 and ECV of noninfarcted myocardium and outcome in patients with coronary artery disease, J. Am. Coll. Cardiol. 71 (7) (2018) 766–778, https://doi.org/10.1016/j.jacc.2017.12.020.